Pergamon

Int. J. Solids Structures Vol. 32, No. 6/7, pp. 767–782, 1995
Copyright © 1995 Elsevier Science Ltd
Printed in Great Britain. All rights reserved
0020–7683/95 $9.50 + .00

0020–7683(94)00159–6

DELAMINATION BUCKLING; EXPERIMENT AND ANALYSIS

JOHN M. COMIEZ, ANTHONY M. WAAS and KHALED W. SHAHWAN

Composite Structures Laboratory, Department of Aerospace Engineering, The University of Michigan, FXB Bldg, Ann Arbor, MI 48109-2118, U.S.A.

(*Received* 1 *February* 1994; *in revised form* 21 *May* 1994)

Abstract—Delamination buckling and growth are failure scenarios that lessen the structural integrity of laminated composite structural members. In the present work a combined experimental and analytical investigation of this failure mechanism in a strictly two-dimensional setting is carried out. When a delamination of an arbitrary planform is present in a structure, the buckling mode of the delamination may involve regions or points of contact with the undelaminated portion of the laminate beneath it. The effect of this physical constraint is investigated by compressing model specimens that contain delaminations of rectangular planform with varying aspect ratio. The shadow Moiré method is used to capture the buckled mode shapes while the results from an approximate analytical model developed elsewhere are used to corroborate the experimental results.

1. INTRODUCTION

Composite materials have found widespread use in industry. In the aerospace industry in particular, these materials have found applications in many secondary structures. At present, there is an effort to use these materials in applications involving load bearing primary structures. In such a case, there is a need to assess the integrity of the structure in the presence of defects. More specifically, once a structural member has been designed, a departure from the "perfect" state of the structure needs to be characterized in terms of residual strength or stiffness.

It is widely accepted that delamination type defects constitute the bulk of damage precipitation in these structures. Bird impact, tool drops, flying runway debris, manufacturing process associated flaws, internal fiber kinking or microbuckling due to excessive internal stresses are some from a variety of situations which culminate in the formation of a delamination (or several of them). If the delaminated portion of the laminate is in a compressive load environment, then delamination buckling and subsequent growth are possible scenarios by which the damage spreads to the undamaged portions of the laminate. Thus, there is a need to assess the residual stiffness of a delaminated laminate under compressive loads without too many restrictions on the shape of the delaminated area as well as the manner in which it grows.

There have been several studies on delamination buckling following the exposition of Chai *et al.* (1981). In their original model, subject to several simplifying assumptions, these researchers showed the importance of studying delamination buckling as a viable mode of failure. Their model development was based on the experimental results obtained via high speed photography coupled with the shadow Moiré technique (Chai, 1982). Since then, many publications on this subject have appeared, and a concise summary of accounts and a long list of references are contained in the work of Davidson (1991)†. In this latter work and the work by Chai (1990), the possibility of the delaminated portion contacting the sublaminate during the buckling and/or subsequent growth has been alluded to, but very few measurements exist to substantiate this claim. In particular, the various factors that give rise to this possibility need investigation. In the event of contact, it is also of interest

† At the time of revising this paper, the authors became aware of another paper (Thouless *et al.*, 1994) that has relevance to the investigation presented here.

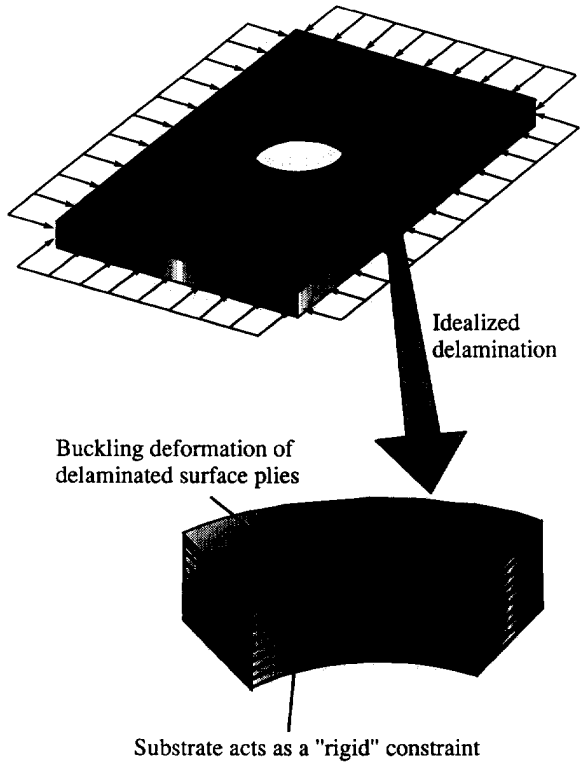

Fig. 1. Schematic of buckled mode shape at edge of a cut-out in a compressively loaded laminate.

to ascertain the change in the stiffness of the delaminated structure and accurately model this change to predict the residual load bearing capacity of the damaged structure.

In the present work, we study model delaminations with rectangular planforms of different aspect ratio, that are placed in a compressive load environment. Our studies are motivated by the interferometric measurements reported in Waas *et al.* (1990), that describes a study on the failure mechanisms of laminates containing cut-outs. In brief, it was found that, subsequent to initial damage formation via fiber microbuckling/kinking, the damage propagated away from the hole edge by a combination of delamination buckling and growth. It was found that the delaminated portions which approximately resembled areas of a part of a sector plate, was found to buckle into a mode shape that at any instant of time during the growth was found to contact with the sublaminate beneath it. A schematic of a buckled mode shape, extracted from the interferograms in Waas *et al.* (1990), is given in Fig. 1.

Model delaminations that have a planform that provides for the possibility of contact is chosen in this study. The results from the experimental study are compared with the results from an analytical study, whose details are presented in Shahwan and Waas (1994). In the remaining sections of this paper, the experiments, choice of specimen, the measurement technique and the results obtained are discussed and compared with the analytical model predictions. Good agreement is found. The post-buckled behavior of the delaminated portion is seen to exhibit some interesting results. The results that are to be presented are novel and provide insight into furthering our understanding on delamination buckling and growth.

2. EXPERIMENTAL WORK

A model experiment that determines the buckling characteristics (buckling load and response shapes) of a delaminated plate while allowing out of plane deflections to occur in one direction only (unilateral) was chosen. The experiment uses an extruded polystyrene

Layer	Properties	Visual Example
Top	**Material:** Transparent Vinyl **Dimensions:** a = 11.5 in b = 4.5 in t = 0.04 in	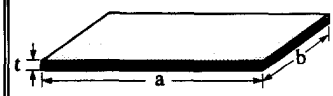
Middle	**Material:** Araldite (Epoxy Structural Adhesive) **Dimensions:** a = 11.5 in b = 4.5 in t = 0.01 in (approx.)	
Bottom	**Material:** Extruded Polystyrene (foam) **Dimensions:** a = 11.5 in b = 4.5 in t = 1.0 in	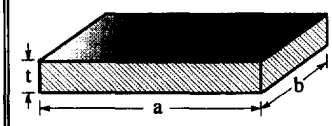

Fig. 2. Summary of the model specimen used in the study.

(substrate) as a foundation for a vinyl plate. The shadow Moiré method is used to visualize the response of the vinyl plate.

2.1. *Experimental details*

The specimen design entailed three layers. The bottom layer (the substrate) acts as a "rigid" foundation and prevents the top layer (vinyl plate) from having any deflection in the negative transverse direction (into the foundation). The top layer is the plate of interest whose buckling characteristics will be determined. The middle layer is a thin epoxy layer. The epoxy bonds the top layer to the bottom layer everywhere except inside the perimeter of the initial delamination planform under consideration, leaving an unbonded region in the middle of the specimen. A summary of the sandwich specimen is given in Fig. 2. Given an external compressive load, this unbonded (delaminated) region will buckle. The substrate and epoxy around the edges of the unbonded region are expected to exert forces and moments which at the first instance may be thought of as being similar in origin to generalized forces exerted by translational and rotational springs.

The shadow Moiré method was used to visualize the response of the unbonded region. In addition, the full-field displacement contours obtained from this method will visually verify the point of buckling during the test.

In selecting a substrate material, the following considerations were employed: the substrate should be made of an isotropic and homogeneous material, and the substrate should have a high bending stiffness as it was desired that the substrate compress in the axial direction only, thus minimizing any out of plane deflections. An additional constraint was the maximum available load of the compression device, at 10,000 lbf. Of a few qualified candidate materials, a 1.0 in thick extruded foamy polystyrene was chosen for its abilities to satisfy all of the conditions and for its ready availability.

Likewise, the following considerations were used in selecting a top layer material: the top layer should be made of an isotropic and homogeneous material, and the combination of bending stiffness, thickness and unbonded region dimensions should not result in a buckling strain that is too small to be accurately measured. A 0.04 in thick solid vinyl was chosen for the top layer material, since it satisfied the above requirements.

The only consideration for the middle epoxy layer is that it should have sufficient strength to allow the top layer vinyl plate to enter the post-buckling region of the test, while allowing no growth of the disbond, prior to buckling. Sample tests showed that Ciba Geigy

Table 1. Material properties for vinyl and polystyrene

Material	Thickness (in)	E (psi)	ν	D (lbf-in)
Solid vinyl	0.04	400,000	0.31	2.34
Extruded polystyrene	1.0	2300	approx. 0.3	210.6

106/953 Araldite fulfilled this consideration. Araldite was chosen for this experiment. The mechanical properties of each layer are given in Table 1.

2.2. *Specimen preparation*

The substrate was cut into pieces that measured 11.5 in × 4.5 in × 1.0 in. Care was taken to ensure that the specimens have the same dimensions as well as perfectly square and parallel edges.

An adhesive reservoir was cut from the substrate at the intended boundary between the bonded and unbonded regions. The purpose of this reservoir is to collect the excess epoxy that is forced into the unbonded region during the bonding process. It is possible that some epoxy may protrude into the unbonded region. If a reservoir is not present, the boundary between the bonded and unbonded region will be erratic. In addition, the unbonded region will become smaller than what was intended.

In actuality, the adhesive reservoir does not collect the epoxy. The epoxy clings to the vinyl plate when it is forced into the unbonded region. With the presence of the reservoir, the epoxy adheres to the vinyl alone, preventing a bond to form between the vinyl plate and the substrate (Fig. 3).

The reservoir was created by cutting a narrow groove into the substrate and around the intended perimeter of the unbonded region. A second rectangle, centered in the unbonded region and slightly smaller was cut. Tweezers removed the substrate between the boundaries of the two rectangles. 0.1 in was chosen for the depth of the reservoir.

Once the reservoir was complete, a hole with a 0.1 in diameter was punched through the center of the substrate. This hole is necessary to release trapped air in the unbonded region when the vinyl plate is bonded to the substrate. Failure to place the hole in the substrate yielded a specimen with an initial imperfection that was of the order of the thickness of the vinyl plate.

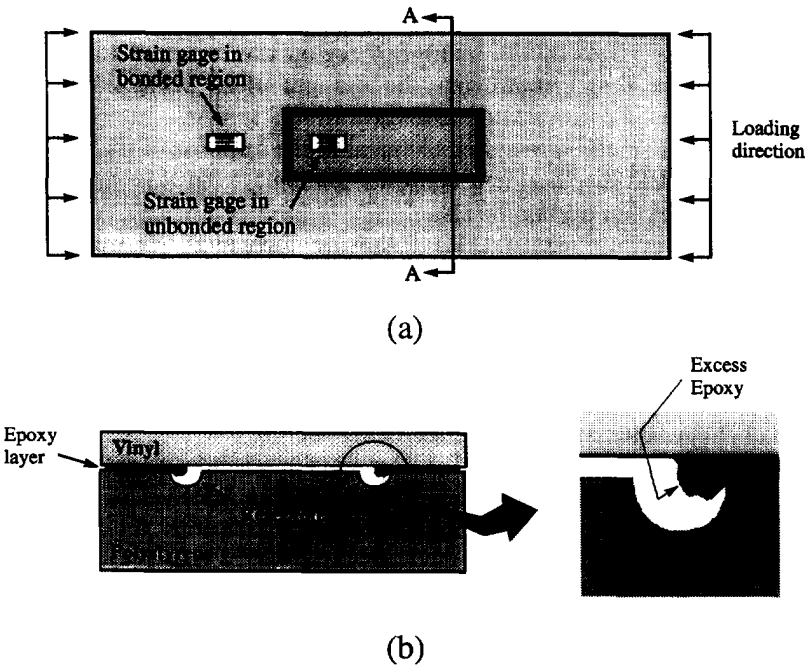

Fig. 3. Details of reservoir and location of strain gages.

In a similar manner as before, 0.04 in thick vinyl was cut into 11.5 in × 4.5 in sections. The cut vinyl plates were spray painted in preparation for use with the shadow Moiré method. However, it must be noted that a compressive force is induced on the vinyl plate when the paint dries up. If the vinyl plate has previously been bonded to the extruded polystyrene, the vinyl plate will be placed under a compressive load as the substrate and epoxy prevent the vinyl from shrinking due to the drying paint. This compressive load produces an out of plane deflection in the unbonded vinyl plate. It is desired that the vinyl plate be as flat as possible, i.e. having an initial imperfection as small as possible. Spray painting the vinyl plate before it is bonded to the extruded polystyrene will result in no initial load on the vinyl plate. The initial imperfection of the vinyl plate was found to be negligible with respect to its thickness.

The final step in the preparation of the specimen was the bonding of the vinyl plate to the substrate. The Ciba Geigy 106/953 hardener epoxy was mixed in the manufacturers suggested 50/50 ratio and spread to a thin and uniform layer onto the intended bonded region of the substrate. The vinyl plate was placed on top of the epoxy and a small roller was used to roll out the air bubbles in the epoxy. Once the air bubbles were removed, the substrate and vinyl plate were compressed together as a sandwich and left to sit for the recommended curing time of 24 hr at room temperature.

After curing, the specimen was removed from its compression. Two strain gages were bonded to the specimen. The first strain gage is located in the unbonded region and the second located in the bonded region (Fig. 3).

2.3. *Test procedure*

A schematic of the test set-up and the optical components for the shadow Moiré method is shown in Fig. 4. The global load, global displacement, surface strain in the bonded region of the specimen, and surface strain in the unbonded region of the specimen is measured with this set-up.

At the commencement of the test, the loading device is programmed to compress the specimen at a crosshead speed of 0.0075 in/min, simulating static conditions. A continuous recording of the out of plane Moiré fringes is effected by the VCR system. For each test, the entire out of plane displacement history of the unbonded region is obtained. In the shadow Moiré method, each of the fringes represents contours of equal out of plane displacements (w). The nth fringe represents a change in w (denoted as Δw) of

$$\Delta w = \frac{\text{grating pitch}}{\tan\alpha + \tan\beta} = \frac{0.005\,\text{in}}{\tan 20^\circ + \tan 40^\circ} = 0.0042\,\text{in} \tag{1}$$

where α and β are as indicated in Fig. 4(b). Thus, with $\alpha = 20^\circ$ and $\beta = 40^\circ$, one fringe spans a change in the out of plane displacement of 0.0042 in. More details of this method can be obtained from Theocaris (1969).

Early tests of the three layered specimen showed an unacceptable amount of specimen bending during the tests. Thus, a specimen support system was manufactured that physically held the four edges of the specimen. These anti-buckling guides prevented the specimen from bending, but allowed axial and transverse contractions and expansions, respectively. It also greatly simplified the test set-up and ensured uniformity between tests. The anti-buckling guides are similar to those used in the experimental work described in Chai (1982).

Prior to each test, the strain gages, LVDT, and load cell were connected to the acquisition system and then balanced and calibrated to account for the pre-strain present due to the shrinking of the spray paint and curing of the epoxy. To measure this pre-strain, a strain gage was bonded to the vinyl plate before it was painted. The strain gage was connected to the acquisition system. Next, the vinyl plate was spray painted and allowed to dry fully while the acquisition system was recording data. With the acquisition system still taking data, the epoxy was applied to the substrate and the vinyl plate was placed on the epoxy. The substrate, epoxy and vinyl plate were lightly compressed as a sandwich. The specimen was then allowed to cure for 22 hr. At this point, the compression was removed

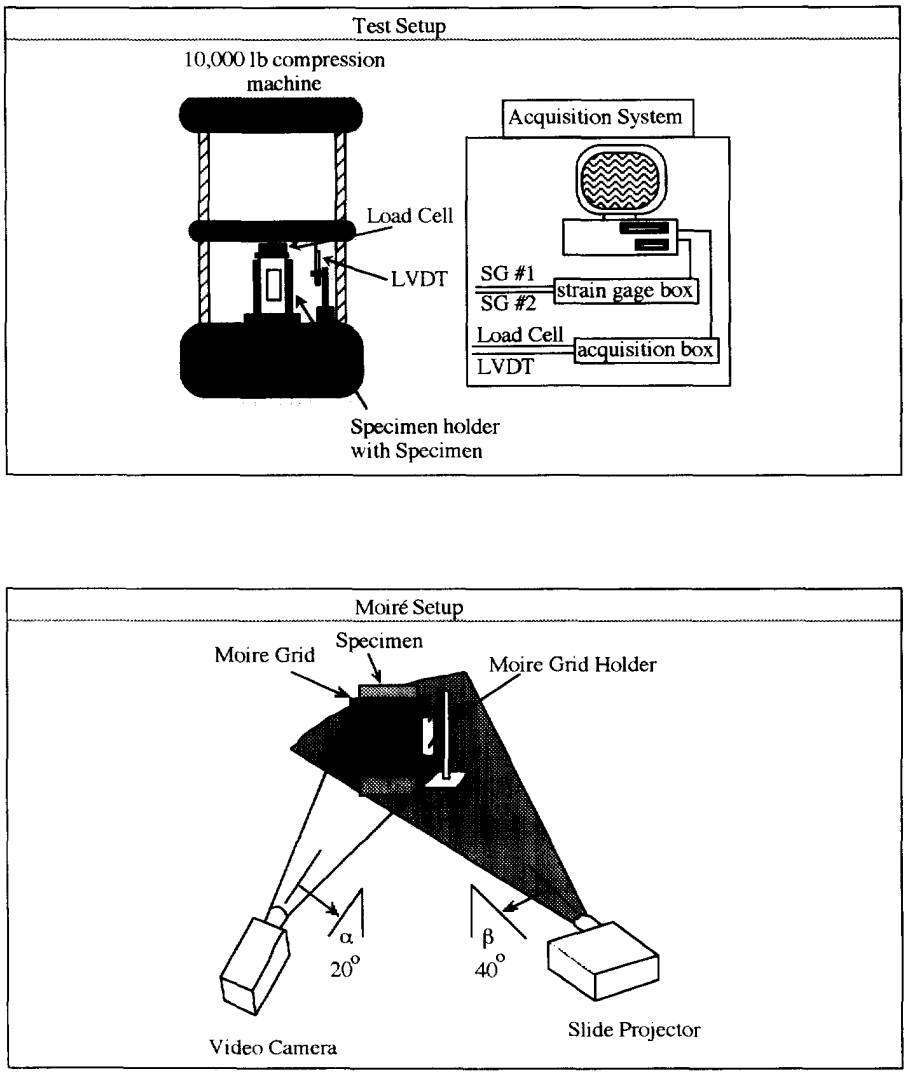

Fig. 4. Schematic of test set-up and shadow Moiré arrangement.

and the specimen was allowed to sit for 2 hrs. The strain in the unbonded region of the vinyl plate was noted. This pre-strain in the vinyl plate was added to the buckling strain of each specimen, as described later.

3. EXPERIMENTAL RESULTS

The spray painting resulted in 48 microstrain of pre-strain in the unbonded region of the vinyl plate. After curing for a total of 24 hrs (after the epoxy had been applied), the strain gage in the unbonded region recorded an additional 264 microstrain. The total pre-strain due to the curing of the spray paint and the epoxy was 312 microstrain. This pre-strain is isotropic, due to its thermal origin. The drying of both the spray paint and the glue is uniform in all directions. For this experiment though, the pre-strain will be assumed to be uniaxial and in the direction of the loading. This is a good assumption because the lowest buckling strain as determined from the tests was just over 3000 microstrain. The pre-strain in the unbonded region is only 312 microstrain. The ratio of the strain at buckling along the length of the unbonded region to the strain at buckling along the width of the unbonded region is about 10 to 1. Thus, this biaxial component is very small with respect to the buckling strain and will therefore be neglected. The aspect ratios of 1, 1.75, 2.5, 3.25, 4 and 5 for the unbonded region were tested. The strain in the bonded region and the strain

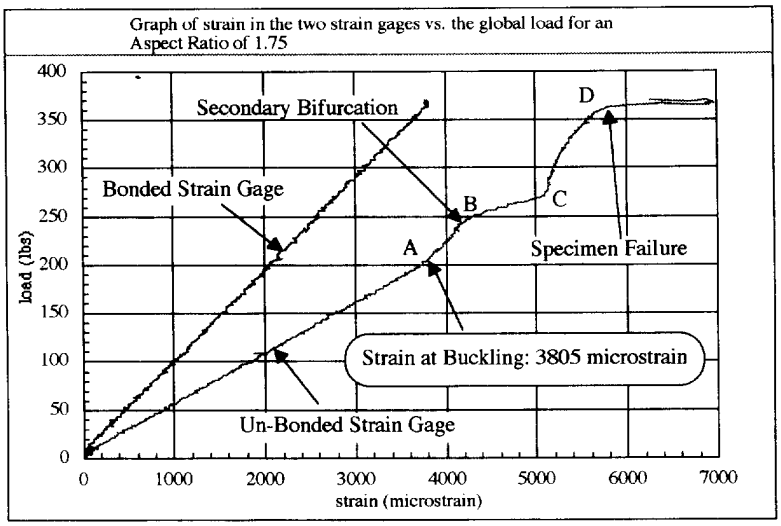

Fig. 5. Plot of strain against applied load for a specimen with $\xi = 1.75$.

in the unbonded region were plotted versus the global load. It should be noted that the global load is the load on the entire substrate, epoxy and vinyl plate system and not the load on the vinyl plate alone. An example of the strain versus load relationship is shown as Fig. 5, for a specimen whose unbonded area conformed to an aspect ratio of 1.75 ($\xi = 1.75$). Certain characteristics of this graph should be noted. As expected, the axial strain (in the direction of load; simply referred to as "strain" for the rest of the discussion) in the unbonded region increases at a constant rate throughout the entire test. The constant loading rate, and thus constant increase of strain ensures that the specimen is undergoing mostly axial compression. The bending of the specimen has been kept at a minimum, with the use of the anti-buckling guides.

The strain in the unbonded regions was more than the strain in the bonded region. This is as expected due to the local stiffness of the middle unbonded section being less than the stiffness of the outside bonded sections.

At 207 lbf, the strain in the unbonded region ceases to increase in a linear fashion. This point has been identified to be the buckling point for the specimen. Investigations of the Moiré fringes for this specimen reveal that the fringes appear immediately after this point in the test indicating that buckling has occurred. Investigation of the strain in the unbonded region after the buckling point shows that the strain increases at a slower rate. The strain gage in the unbonded region measures the strain on the top surface of the vinyl plate. At buckling, the bending of the vinyl plate relaxes the top surface compressive strain while the bottom surface of the vinyl plate undergoes an increase in compressive strain. The strain, as read by the strain gage on the top surface of the vinyl plate, is relieved as buckling occurs resulting in a drop in the rate of increase of strain (segment AB in Fig. 5). At 250 lbf, the vinyl plate underwent another change in mode shape. The post-buckling of a unilaterally constrained plate turns out to be progressive. The plate does not start flat and then, at the buckling load, respond into its buckling mode. Instead, the plate starts flat and at the buckling load, one hump localized somewhere along the length of the plate starts to appear. Some time after, a second hump will appear. Then a third will appear and so on, until all the humps comprising a stable response mode have shown up. This results in a permanent post-buckled mode shape that the plate responds in prior to growth of the disbond. Notice that at the time at which the second hump starts to form, the strain gage in the unbonded region records a drop in the rate of increase of strain. The reason for this is that the strain gage in the unbonded region is located on the first hump. The formation of the second hump reduces the out of plane deflection of the first hump. With the amount of bending of the first hump reduced, there is an increase in the rate of strain as recorded by the strain gage (segment BC, Fig. 6).

At 268 lbf, the specimen has reached its final post-buckled response shape. The unbonded region has now developed into a stable post-buckled profile with no further changes in geometry. At this point, the stiffness of the system is at its greatest (segment CD, Fig. 5). Unlike bilateral (unconstrained) buckling, the stiffness of the system increases after buckling. This is due to the contact points that arise between the unbonded region and the substrate. This contact increases the axial stiffness of the entire system.

At 360 lbf, the specimen underwent a global failure. In this particular test, the vinyl plate debonded from the substrate along the boundary between the bonded and unbonded regions.

Examples of the concepts listed above will now be given using a set of Moiré fringes which were taken from several tests. The first set of fringes is from a test where the unbonded region aspect ratio(ξ) is 2.5 as shown in Fig. 6. The first set of fringes in this figure shows that the initial imperfection of the plate is negligible, since there is only one fringe and it covers the entire plate. This was the case in all of the specimens that were tested.

The second set of fringes shows one hump starting to form at a global load of 201 lbf. Note that during the test, all of the plates underwent a small amount of bending and twisting. This is shown by the perimeter fringes that appear in these photos.

At a load of 273 lbf, the plate undergoes a change in buckle mode shape. The next set of fringes (labeled as picture 3; similar labels are used for the remainder of this paper) shows the single hump which has grown larger just prior to this instability. Figure 7, which shows the next five sets of fringes (and the final set of fringes from the previous figure) pertaining to this instability, are consecutive frames, 1/30th of a second apart, taken off the videotape of the test. Picture 3 shows the single hump which has grown larger (the last set of fringes in Fig. 6). 1/30th of a second later, the next frame shows a second hump starting to appear in the form of a blurry patch (picture 4). The next frame shows a single fringe on the second hump (picture 5). The next frame shows two complete fringes for the second hump (picture 6). In the next frame, the plate ceases to be unstable with two fringes in the second hump (picture 7). The second hump then grows slowly. At 318 lbf, the second hump has reached a larger size (picture 8). Shortly after this point, the plate undergoes a global failure, in the form of disbond growth, at a load of 320 lbf (picture 9). In this case, the vinyl plate debonds from the substrate at the boundary between the bonded–unbonded regions.

Investigation into another test ($\xi = 4.0$) reveals more characteristics of this unilateral buckling problem, which are shown in Fig. 8. The first set of fringes for this test (picture 10) shows what appears to be two humps forming at a global load of 160 lbf. In actuality the fringe on the left is a valley instead of a hump. This is shown better in picture 11. At 172 lbf, two humps can be seen with a valley in between. This valley is a region where the vinyl plate has come in contact with the substrate below. This contact area is of great interest since it is unique to unilateral buckling problems. Picture 12 shows the two initial humps maturing while a third hump starts to form at 243 lbf. This set of fringes also clearly shows the contact region between the two initial humps and the beginning of a contact region between the middle hump and the right one. The final picture for this aspect ratio (picture 13) shows that all three humps have matured as well as the three contact regions at a load of 357 lbf.

Just as mode shapes in unconstrained plate buckling problems, the mode shapes in unilaterally constrained plate buckling problems are also dependent on the aspect ratio of the plate in question. An aspect ratio of 2.5 has been shown to result in a two hump response. An aspect ratio of 4.0 has been shown to result in a three hump response. A picture of the final buckling response for an aspect ratio of 5.0 shows a four hump response at a global load of 341 lbf, as indicated in Fig. 9. Unfortunately, for the aspect ratio of 5.0, part of the fringe patterns were cut out of the picture since the Moiré grid was only 6.0 in in length while the unbonded length was 7.5 in. But, this picture still shows many of the important points that have been made. First, the shadow Moiré method produced very clear and illustrative fringe patterns that are reflective of the buckling modes. Second, from the fringes, it can be deduced that the contact regions are very prevalent between each of the humps. It is not known if there were contact points between the humps on the far ends

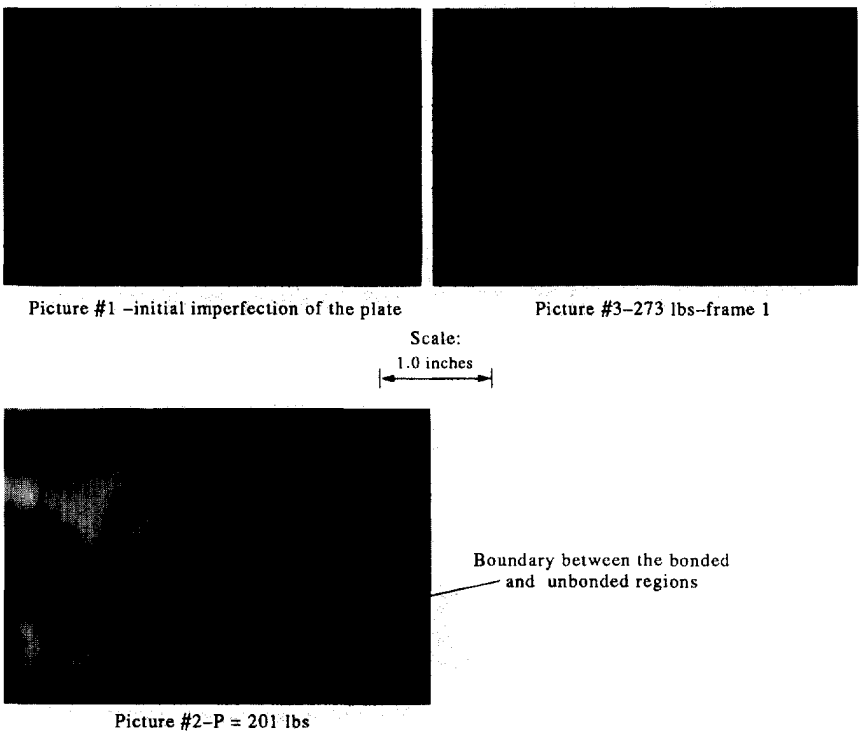

Fig. 6. Moiré fringes for a specimen with $\xi = 2.5$, showing buckle initiation.

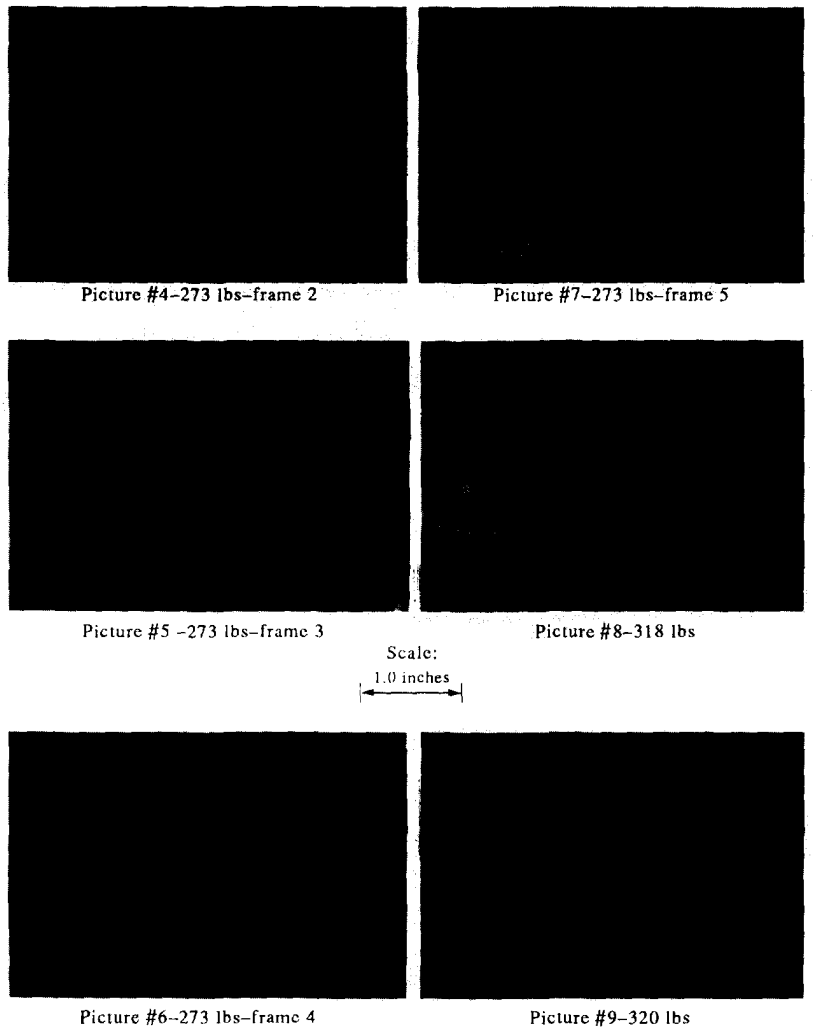

Fig. 7. Moiré fringes for a specimen with $\xi = 2.5$, showing buckle formation and final failure by delamination growth.

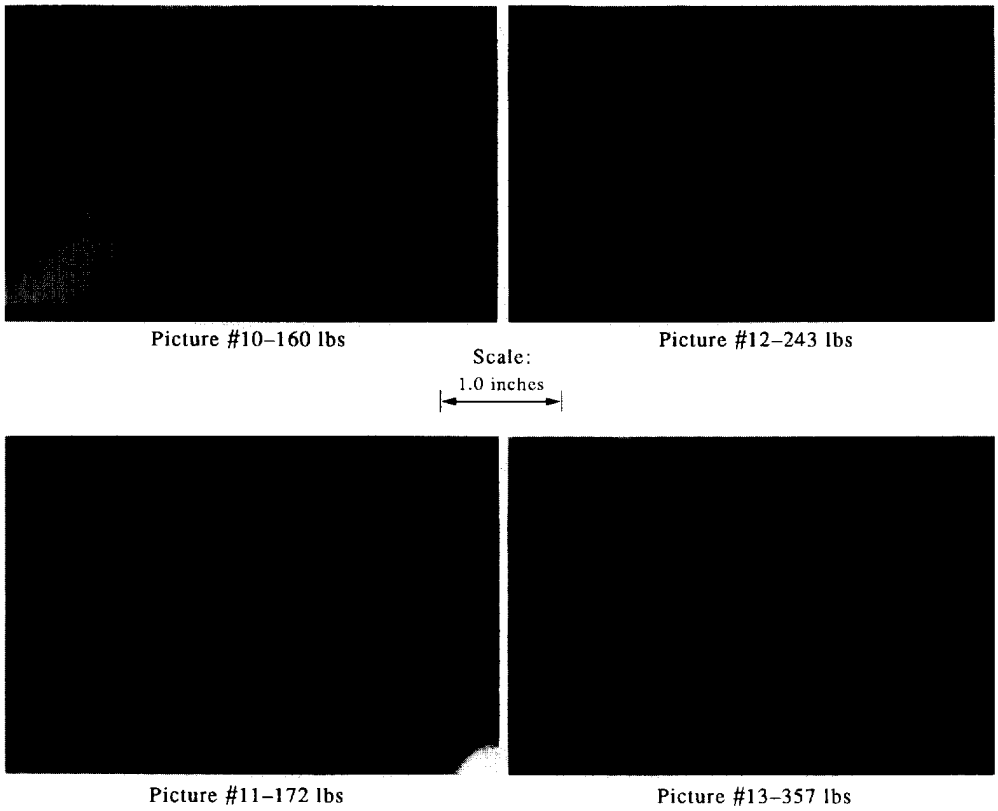

Fig. 8. Sequence of Moiré fringes for a specimen with $\xi = 4.0$, showing various stages of buckle development.

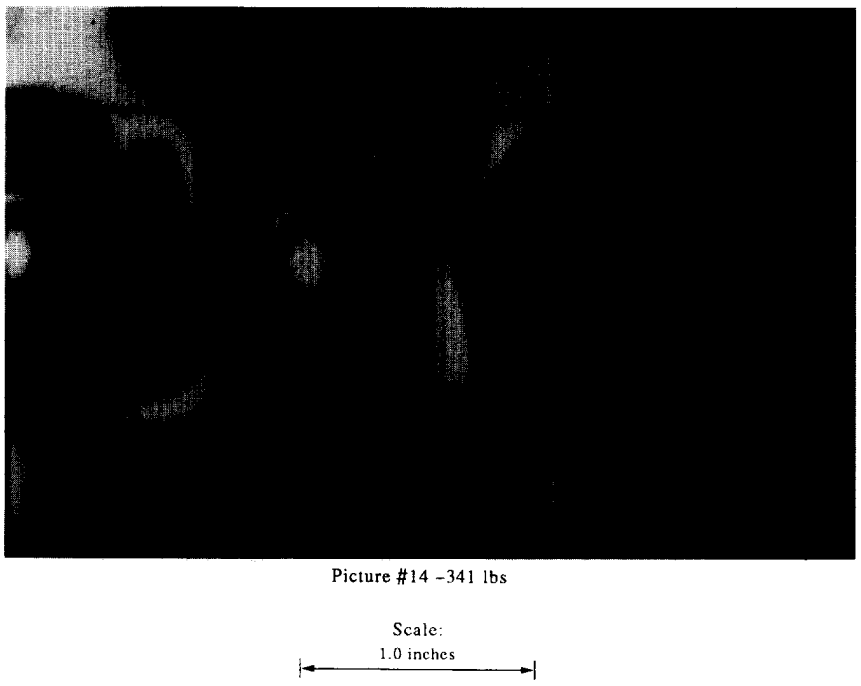

Fig. 9. Moiré fringes of buckle mode shape for a specimen with $\xi = 5.0$. Notice the relatively flat regions between the humps.

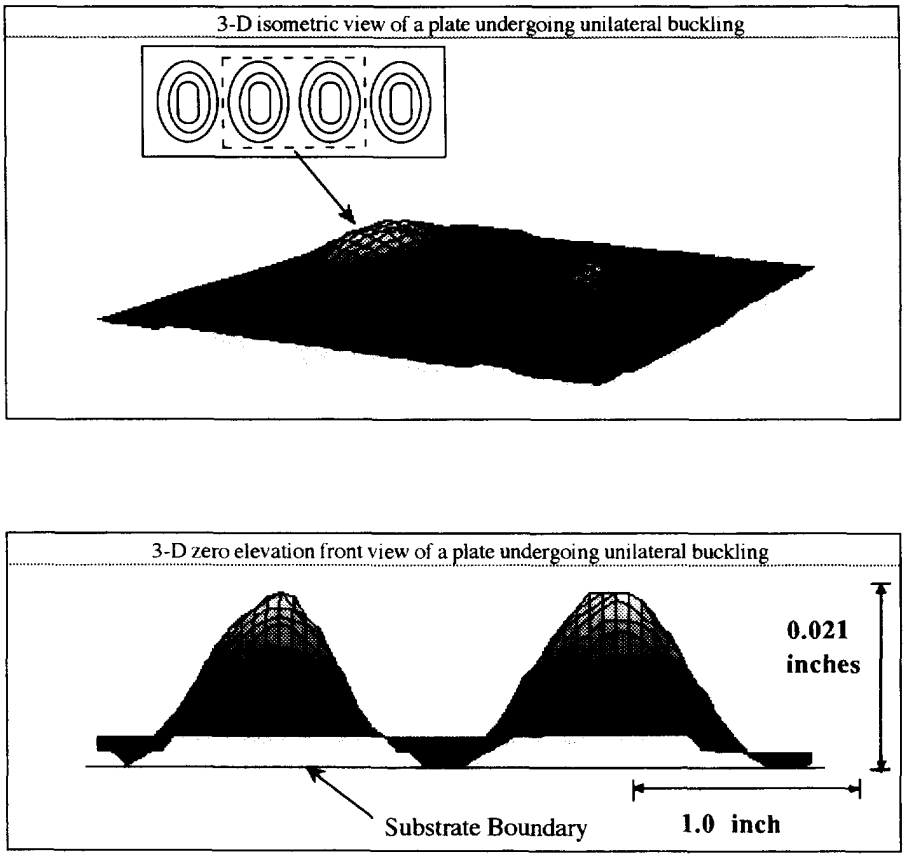

Fig. 10. Typical displacement profiles corresponding to the Moiré fringes discussed.

of the plate. A three-dimensional reconstruction created from data for a test on an aspect ratio of 5, is shown in Fig. 10. Since the buckling pattern is periodic, only two of the humps are shown in the re-creation. For clarity the vertical scale is exaggerated in this re-creation. Also shown in this figure is a zero elevation front view. This figure also shows the contact regions (for clarity the vertical scale is exaggerated in this figure). The right hump in this picture appears to have a flat top. In actuality, it doesn't. This flat region is due to the coarse fringe density. Again, notice the contact regions. These figures also show the right hump to be smaller than the left one; this is due to the progressive nature of the buckle formation in this problem. In this case, the left hump formed and matured earlier than the right one.

The features described in the first three scenarios were very typical of all the tests that were performed. In addition, the aspect ratio of 2.5 was chosen to investigate the repeatability of the tests. This aspect ratio was tested three times. The buckling strain values for these tests were within 4% of each other. It can be concluded that the tests are repeatable. A summary of the results obtained in the six tests is given in Table 2.

Table 2. Summary of buckling test results

Aspect ratio	Strain at buckling	Initial pre-strain	Total buckling strain	Buckling coefficient
1.0	4550	312	4862	7.56
1.75	3805	312	4117	6.41
2.5	3380	312	3692	5.74
3.25	3260	312	3572	5.56
4.0	3085	312	3397	5.29
5.0	3115	312	3427	5.33

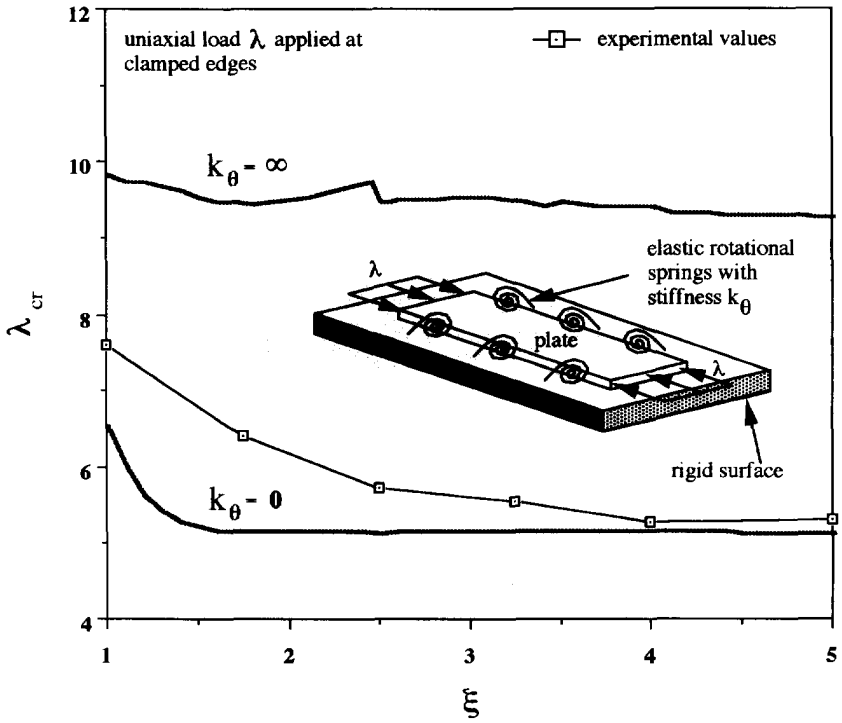

Fig. 11. Comparison of experimentally determined buckling coefficients with predictions of an approximate model (see also Shahwan and Waas, 1994).

In order to compare the results thus obtained with those of an analytical model prediction, the results for the buckling coefficients as a function of aspect ratio is plotted in Fig. 11. Prior to discussing these results, a brief overview of the analysis is appropriate.

4. ANALYSIS

Most of the details that are pertinent to the analysis is omitted here. The reader is referred to Shahwan and Waas (1994) for completeness. In the analysis, in order to account for the physical constraint imposed on the plate's buckling displacements, a nonlinear elastic foundation model that exhibits a deformation sign dependent force–displacement relationship was implemented. Such types of nonlinearities present analytical difficulties in that an exact close-form solution cannot be easily obtained, if not impossible. As such, an approximate method of solution was followed to formulate the equations governing the plate's response. From the expression of the total potential energy and setting its first variation to zero the governing equilibrium equations were derived. These were next approximately solved using Galerkin's method. In order to carry out the solution procedure, kinematically admissible global displacement functions must be assumed. It is important to note that although the plate is unilaterally constrained, such a constraint does not play any role in choosing these functions. Instead, this constraint condition was accounted for indirectly via the nonlinearity of the elastic foundation model. Further, the out of plane displacement field w was assumed to be of a separable form where shape functions in x are multiplied by those in y. These functions were chosen to be the buckling and/or free vibration eigenmodes of beams and/or plates having the same kinematic boundary conditions [see Shahwan and Waas (1994)]. The solution of the resulting nonlinear algebraic equations was carried out in an incremental fashion by ramping the in-plane load parameter and monitoring the determinant of the incremental stiffness matrix. The critical value of the far-field load was obtained when the incremental stiffness matrix became singular (or near singular). Such an approach is used frequently in the analysis of nonlinear problems.

The type of foundation model needed to incorporate the physics of unilaterally constrained plates should exhibit a force–displacement relationship that is deformation sign

dependent, hence, the foundation was modeled as extensional springs having such a relationship. Such models have been considered by many investigators in the treatment of beams and plates resting on nonlinear foundations (Tsai and Westmann, 1967; Farshad and Shahinpoor, 1972; Celep, 1988). In these studies, the sign, Dirac delta as well as Heaviside step functions were used to describe the bimodulus nature of the elastic foundation (bimodulus in the sense that compression stiffness is different from that for tension). In this study, a model that utilizes the switching property of the tanh function was used. The force–displacement relationship for this model is given below as

$$F = \alpha\Psi(w) \tag{2}$$

where

$$\Psi(w) = w\,[\tfrac{1}{2}(1-\tanh(\beta w))], \tag{3}$$

F is the force in a spring, α is a non-dimensional stiffness parameter, w is the normalized deformation, β is a spring (foundation) attachment coefficient that is >0. The foundation attachment can be controlled by changing the value of the parameter β. Large values of β imply less attachment. Theoretically, $\beta = \infty$ implies that the foundation is fully unattached (tensionless), while $\beta = 0$ implies that the foundation is fully attached (note that if $\beta = 0$, the $\frac{1}{2}$ factor in eqn (3) should be replaced by 1 in order to recover the linear case where $\Psi = w$). Furthermore, while foundation stiffness can be increased to larger values by increasing α, increasing β will result in a decrease in the ratio of the tension/compression stiffnesses.

It is worthwhile noting that although the nonlinearity in the physical problem is geometrical, arising from the constraints imposed on the plate's behavior, the nonlinearity in the governing equations arose from the elastic foundation's constitutive model. Notice that this is a feature of the mechanical model that is employed in the analysis.

The analytical model prediction is plotted against the experimental results as shown in Fig. 11. Two bounds from the analysis are indicated. The upper bound corresponds to the case where the unloaded disbond edges are clamped. The lower bound corresponds to the case where it is assumed that these edges are simply supported. For the case of unloaded edges clamped (marked in figure as $k_\theta \to \infty$), the solution exhibits discontinuities as a function of plate aspect ratio (ξ). These discontinuities can be attributed to the fact that in the neighborhood of the particular ξ value corresponding to the discontinuity, topological changes in the buckle patterns occur. Such changes were drastic in the neighborhood of $\xi = 2.5$.

As is clearly seen from Fig. 11, the experimental results fall right between the upper and lower bounds, but closer to the lower bound. This is as expected, since at the disbond/bonded boundary, the delamination is neither clamped nor simply supported but is very likely to be best modeled as being supported by rotational and transverse springs. It must be noted that in the experiment, the response of the disbond formed gradually, except in some cases where the disbond "snapped" from a perfectly flat state to one that is buckled, characteristic of a true bifurcation. This happened only for the very small aspect ratio plates. To some extent, this is not surprising, since the corresponding unconstrained buckling problem for plates of small aspect ratio yield buckling modes that are of one sign, whereas for larger aspect ratio plates, the buckle mode contains more than one half wave along the length.

5. CONCLUDING REMARKS

Delamination buckling and growth are important failure mechanisms that degrade the structural integrity of composite laminated structural members. In the present work a combined experimental and analytical approach was employed to study this failure mode in a two-dimensional setting employing some model delaminated structural plates. As noted by Chai (1990) and analysed in Shahwan and Waas (1994), it was found that the buckling

mode of the delamination may involve regions or points of contact with the undelaminated portion of the laminate beneath it. The effect of this physical constraint was shown to cause the response of the delaminated portion to occur in a progressive fashion. The shadow Moiré technique that was employed was able to clearly show that the mode shape was periodic and contained points and/or regions of contact. A simple and approximate mechanical model was used to compute results for the buckling loads which were found to bound the experimental values. It is clear that the stiffness of a post-buckled delaminated plate is highly influenced by whether the buckled portion involves points or regions of contact or not. Thus, in analytical model development, the possibility of the delaminated portion contacting the plate cannot be excluded. Instead, the corresponding buckling problem must be addressed within this wider setting that incorporates the possibility of contact. The resulting boundary value problem solution should then deliver the result whether contact occurs or not.

Acknowledgements—We are thankful for the financial support from the Horace Rackham Graduate School, University of Michigan and the partial funding from the ONR Mechanics Division. Dr Yapa D. S. Rajapakse served as the Scientific Officer from ONR.

REFERENCES

Celep, Z. (1988). Rectangular plates resting on tensionless elastic foundations. *J. Engng Mech.* **114**(12), 2083–2092.

Chai, H. (1982). The growth of impact damage in compressively loaded laminates. Ph.D. thesis, Caltech, Department of Aeronautics.

Chai, H. (1990). Buckling and post buckling behavior of elliptical plates. Parts I and II: analysis and results. *J. Appl. Mech.* **57**, 981–994.

Chai, H., Babcock, C. D. and Knauss, W. G. (1981). One dimensional modeling of failure in laminated plates by delamination buckling. *Int. J. Solids Structures* **17**, 1069–1083.

Davidson, B. (1991). Delamination buckling: experiment and theory. *J. Compos. Mater.* **25**, 1351–1378.

Farshad, M. and Shahinpoor, M. (1972). Beams on bilinear elastic foundations. *Int. J. Mech. Sci.* **14**, 441–445.

Shahwan, K. and Waas, A. M. (1994). A mechanical model for the buckling of unilaterally constrained rectangular plates. *Int. J. Solids Structures* **31**(1), 75–87.

Theocaris, P. (1969). *Moiré Fringes in Strain Analysis*. Pergamon Press, Oxford.

Thouless, M., Jensen, H. M. and Liniger, E. G. (1994). Delamination from edge Flaws. To appear in *Proc. R. Soc. London*.

Tsai, N. and Westmann, R. (1967). Beams on tensionless foundation. *J. Engng Mech. Div.* **93**, 1–12.

Waas, A. M., Babcock, C. D. and Knauss, W. G. (1990). An experimental study of compression failure of fibrous laminated composites in the presence of stress gradients. *Int. J. Solids Structures* **26**(9/10), 1071–1098.